High Temp. Mater. Proc., Vol. **31** (2012), pp. 27–35 DOI 10.1515/HTMP.2011.125

Influence of Processing Route and Section Size on Elevated Temperature Tensile Properties of 9Cr-1Mo Ferritic Steel

Binod Kumar Choudhary[1,*]

[1] Mechanical Metallurgy Division, Indira Gandhi Centre for Atomic Research, Kalpakkam, India

Abstract. Tensile tests were performed on specimens obtained from 20 mm plate in normalised and tempered condition and quenched and tempered thick section tubeplate forging to assess the influence of processing route and section size on room and elevated temperatures (300–873 K) tensile properties of 9Cr-1Mo ferritic steel. Yield and ultimate tensile strength values of plate and tubeplate forging exhibited a gradual decrease up to intermediate temperatures followed by a rapid decrease at high temperatures. Ductility values displayed a gradual decrease to a minimum at intermediate temperatures followed by an increase at high temperatures. The fracture mode remained transgranular. At intermediate temperatures, 9Cr-1Mo steel in both the product forms exhibited similar serrated flow, an important manifestation of dynamic strain ageing. At all temperatures, thick section tubeplate forging exhibited lower strength and higher ductility values compared to normalised and tempered steel. The inferior strength values were attributed to coarse microstructure of the forging.

Keywords. Ferritic steel, tubeplate forging, tensile properties, coarse lath martensite, serrated yielding.

PACS®(2010). 62.20 F-, 81,40.Lm, 62.20.D-, 81.40.Jj.

1 Introduction

Ferritic 9Cr-1Mo steel and its modified versions are important high temperature materials for steam generator (SG) applications in fossil-fired thermal power and nuclear power plants. The steel also finds use in chemical, petrochemical and fertiliser industries. The choice of 9Cr-1Mo steel for steam generator applications is based on the low thermal expansion coefficient and high resistance to stress corrosion cracking in water-steam systems compared to austenitic stainless steels, in addition to better mechanical properties at elevated temperatures compared to alternate 2.25Cr-1Mo steel [1–3]. Apart from good weldability and microstructural stability, the steel also offers a good combination of high creep strength and ductility over long exposures [1–3]. Due to high hardenability, 9%Cr steels display the ability and tolerance to offer nearly constant microstructure over large section size, which in turn provides only small variations in mechanical properties with increasing thickness, and between surface and the centre of thick section products [4]. In the steam generators of sodium cooled fast breeder reactor (SFRs), thick section tubeplate together with tube and shell are manufactured using either 9Cr-1Mo or modified 9Cr-1Mo steel. Use of single structural material in steam generators enhances the reliability of the components including critical tube to tubeplate welds. 9%Cr steels has also emerged as an important candidate material for wrapper applications in future SFRs due to high resistance to irradiation creep and void swelling compared to austenitic steels [5, 6]. Austenitic steels used for wrapper application suffer from bowing of subassemblies due to differential void swelling and this result in severe handling problems thereby restricting the fuel burn up. In order to overcome this problem, 9%Cr ferritic steel has been chosen as an alternate and is being developed for wrapper applications.

Present study is aimed at comparative evaluation of room and elevated temperatures tensile properties of 9Cr-1Mo steel in two different product forms i.e., normalised and tempered ($N + T$) 20 mm plate material and thick section tube plate forging of 1000 mm diameter and 300 mm thickness in quenched and tempered ($Q + T$) condition. Elevated temperature tensile properties are one of the important considerations for the design of steam generator components and the evaluation of tensile properties forms the first step towards characterisation of materials performance for high temperature application. 9% Cr steel exhibits a gradual decrease in strength values up to intermediate temperatures followed by rapid decrease at high temperatures [1,3]. Investigation on a wide range of simulated heat affected zone microstructures [7] have indicated that fine grain structure exhibits a good combination of strength and ductility. Therefore, fine grain structure is desirable in 9Cr-1Mo steel. Based on the influence of heat treatments intended to simulate microstructures of thick section products, it has been shown that simulated thick sections display inferior tensile strength compared to that of thin section bar material [4]. Due to paucity of information on the elevated temperature mechanical properties of actual thick section products as

* **Corresponding author:** Binod Kumar Choudhary, Mechanical Metallurgy Division, Indira Gandhi Centre for Atomic Research, Kalpakkam 603 102, Tamil Nadu, India; E-mail: bkc@igcar.gov.in.

Received: April 6, 2011. Accepted: June 12, 2011.

Product form	Element (wt.%)							
	C	Cr	Mo	Si	Mn	S	P	Fe
20 mm plate	0.10	8.44	0.95	0.48	0.45	0.002	0.008	Balance
Tubeplate forging	0.10	9.27	1.05	0.75	0.63	0.001	0.02	Balance

Table 1. Chemical composition (wt.%) of 9Cr-1Mo steel.

well as the absence of realistic estimate for the variations of tensile properties with section size, tensile properties were evaluated in two product forms of thin section $N + T$ plate and thick section tubeplate forging of 9Cr-1Mo steel. The tensile properties of plate material and tubeplate forging are examined in terms of the variations in strength and ductility values with temperature. The strength and ductility values obtained for thick section tubeplate forging have been compared with the respective values obtained for $N + T$ plate steel. The variations in tensile properties are discussed in terms of the influence of heat treated microstructures obtained in two different forms of the steel.

2 Experimental

9Cr-1Mo steel in two different forms i.e., plate of 20 mm thickness and thick section tubeplate forging of size 1000 mm diameter and 300 mm thickness were used in this study. The chemical composition of the two steels is given in Table 1. 9Cr-1Mo steel plate of 20 mm thickness in normalised and tempered condition was supplied by Creusot-Loire industries, France. The plate processed by hot rolling was normalised at 1223 K for 15 min followed by air cooling and tempered at 1053 K for 2 h followed by air cooling. 1000 mm diameter and 300 mm thick tubeplate forging in quenched and tempered ($Q + T$) condition was supplied by BRUCK, GmbH, Germany. The hot forged tubeplate was austenitised with controlled heating (heating time 8 h) to 1223 K and soaking at 1223 K for 5 h followed by quenching in water. Tempering treatment involved controlled heating (heating time 8 h) to 1023 K and soaking at 1023 K for 8 h followed by air cooling. Specimen blanks of 12 mm diameter and 60 mm length were machined with stress axis in the rolling direction from the $N + T$ plate material. In case of $Q + T$ tubeplate forging, 12 mm diameter and 60 mm long specimen blacks were machined with stress axis in the thickness direction from the outer annulus of 300 mm width. Cylindrical button head tensile specimens with a gauge diameter of 4 mm and gauge length of 26 mm were machined. Tensile tests were carried out in air in a floor model Instron 1195 universal testing machine equipped with a three-zone temperature control furnace and a stepped-load suppression unit. Tests were performed on $N + T$ plate and $Q + T$ forged tubeplate specimens over a temperature range 300–873 K at nominal strain rate of 1.26×10^{-3} s^{-1}. Temperatures in all the tests were controlled within ± 2 K. Load-elongation curves were recorded using the Instron autographic recorder for all the tests. Use of suitable chart speed gave a strain resolution of 7.5×10^{-4} and stepped zero suppression gave a stress resolution of 0.80 MPa.

True stress (σ)-true plastic strain (ε) data were obtained using a computer program from the digitized load-elongation data up to the maximum load values. Since, no strain gauge was employed, the cross head displacement was taken as the specimen extension. The linear elastic portion of load-elongation data was contributed by the specimen, machine frame, and load-train assembly. The combination of this elastic elongation was subtracted from the total elongation by appropriately using the slope of the initial linear portion of the load-elongation curves for the calculation of plastic strain. Stress and plastic strain data were used to determine true stress (σ)-true plastic strain (ε).

Metallographic examinations on as-received $N+T$ plate and $Q+T$ tubeplate specimens were carried out in a Richert MeF_2 optical microscope equipped with a camera. Specimens were prepared using standard metallographic techniques and by immersion etching in Vilella's reagent (1 g picric acid +5 ml HCl + 100 ml ethyl alcohol). Fractographic examinations on tested specimens were performed using Camscan 3200 scanning electron microscope (SEM).

3 Results

3.1 Microstructure

The microstructure obtained for $N + T$ plate material is shown in optical micrograph in Figure 1. The microstructure consists of fine tempered lath martensite and fine precipitates. The boundaries of prior austenite grains and martensite laths were decorated with precipitates and the intralath matrix regions contained a large number of fine precipitates. The microstructure for $Q + T$ tube plate forging was composed of tempered lath martensite and a few stringers of pro-eutectoid ferrite at prior austenite grain boundaries (Figure 2a). Pro-eutectoid ferrite was estimated to be $\sim$2% by point count method. No significant difference in the amount of pro-eutectoid ferrite was noticed between the surface/sub-surface regions and along the thickness within 300 mm annulus of the forging. The boundaries of prior austenite grains, martensite laths and pro-eutectoid

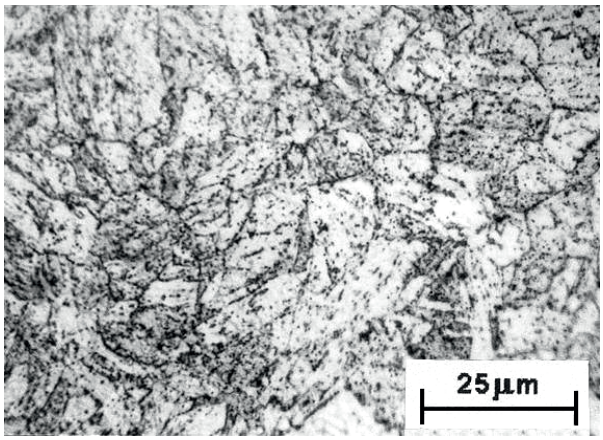

Figure 1. Microstructure of normalised and tempered 9Cr-1Mo steel showing tempered lath martensite and precipitates on grain and lath boundaries and in the matrix region.

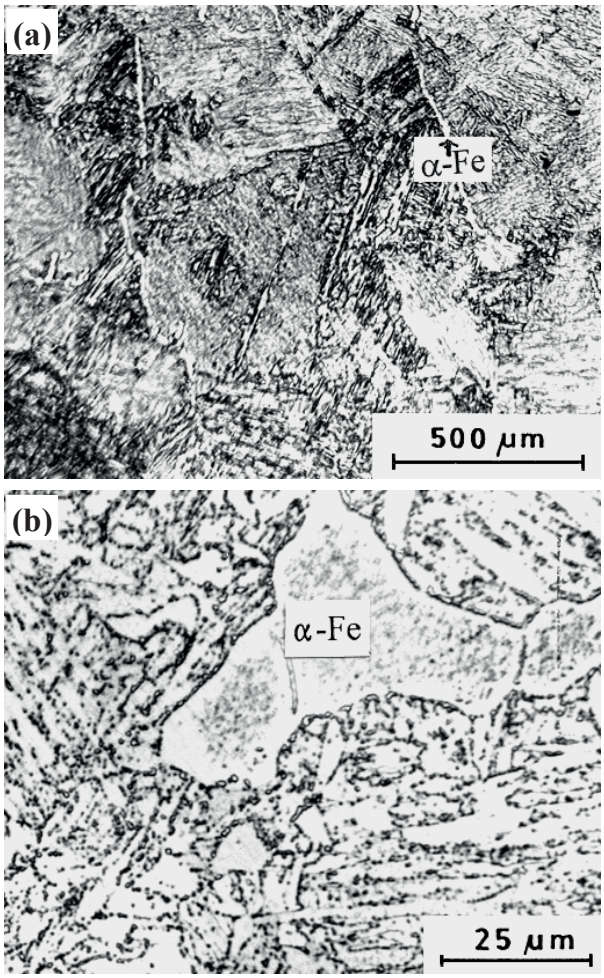

Figure 2. Microstructure of 9Cr-1Mo steel tube plate forging showing (a) tempered lath martensite and pro-eutectoid ferrite as stringers at prior austenite grain boundaries and (b) coarse precipitates on grain, lath and ferrite boundaries and in the matrix region.

ferrite were decorated with coarse precipitates (Figure 2b). The intralath matrix and pro-eutectoid ferrite regions contained large number of fine precipitates. Average prior austenite grain size measured by linear intercept method was ∼25 µm for $N + T$ 20 mm plate material. Tubeplate forging exhibited coarse prior austenite grain size of 120 µm. In addition to coarse austenite grain size, tubeplate forging exhibited coarse lath martensite and packet size and coarser precipitates compared to those displayed by $N + T$ plate material (Figures 1 and 2). X-ray diffraction analysis of bulk precipitates extracted from heat treated specimen revealed presence of $M_{23}C_6$ ($[Cr,Fe]_{23}C_6$) and M_2X (Cr_2N) precipitates. It has been reported that the precipitates present at lath and prior austenite grain boundaries to be $M_{23}C_6$ carbides rich in chromium, whereas intralath matrix regions contain fine M_2X i.e., Cr_2N precipitates [8–11].

3.2 Serrated Load-Elongation Curves

The load-elongation curves at room and high temperatures were smooth. At intermediate temperatures, serrated (jerky) load-elongation curves were observed for both $N + T$ plate and $Q + T$ tubeplate forging. The segments of various types of serrations observed at the strain rate of 1.26×10^{-3} s^{-1} for $N + T$ plate and $Q + T$ tubeplate forging are shown in Figures 3 and 4, respectively. Based on the classification of serrations [12–15], the different types of serrations observed during tensile deformation in 9Cr-1Mo steel can be classified into type A, B or C serrations. For $N + T$ plate steel, mild irregularity at 523 K followed by type A serrations at 548, 573 and 598 K, and mixed type A + B serrations at 623 and 648 K were observed with increasing temperature (Figure 3). Type A serrations results from the diffusion of solute atoms to mobile dislocations arrested temporarily in the slip path. During waiting time, a critical composition of solute atoms around the dislocations is attained, which lock the dislocations. The sharp rise in load before a discontinuous drop is due to solute locking of mobile dislocations and the load drop results from the unlocking of dislocations from the atmosphere. The repeated locking and unlocking of mobile dislocations give rise to serrated load-elongation curve. In general, type A serrations show abrupt rise in the load followed by load drops to either general level of load-elongation curves or below general level of load-elongation curves. The initiation of type B serrations results from locking of mobile dislocations in the propagating type A bands. The onset of type B serrations in the propagating type A bands occur either after occurrence of few pure type A serrations at high strains or right from the beginning of serrated yielding giving rise to mixed type A + B serrations. Type B serrations oscillate about the mean load values, i.e., the general level of load-elongation curves. Unlocking type C serrations characterized by load drops always below the general level of load-elongation curves were observed at 623 K. At the high-

Product form	Type of serrations at different temperatures (K)							
	523	548	573	598	623	648	673	698
20 mm plate	Irr	A	A	A	A+B	A+B	C	Irr
Tube plate forging	A	A	A	A+B	A+B	A+B	C	Irr

Irr – Irregularities

Table 2. Serrations at various temperatures in 9Cr-1Mo steel at strain rate of 1.26×10^{-3} s^{-1}.

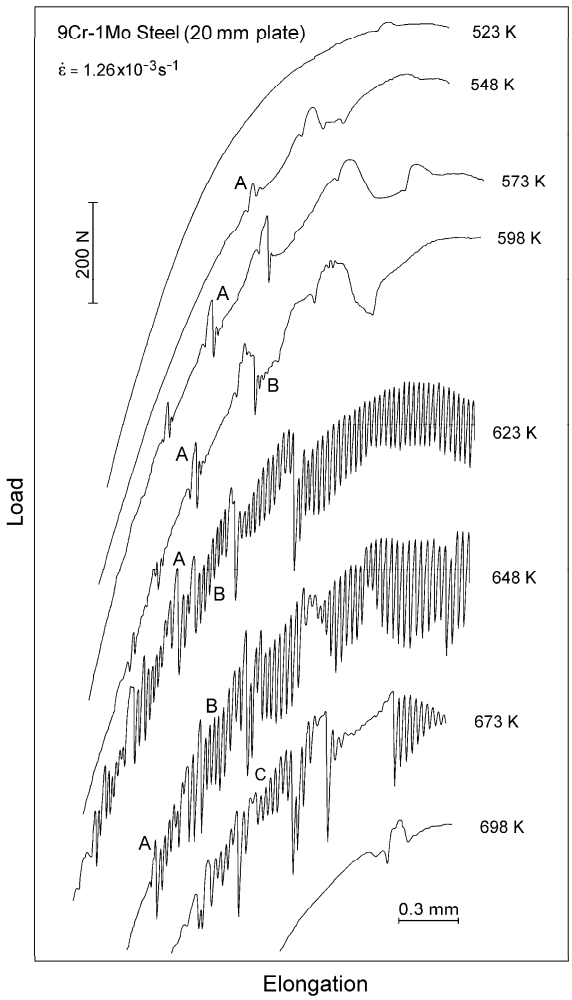

Figure 3. Segments of load-elongation curves showing serrated flow for normalised and tempered specimens tested at various temperatures at a strain rate of 1.26×10^{-3} s^{-1}.

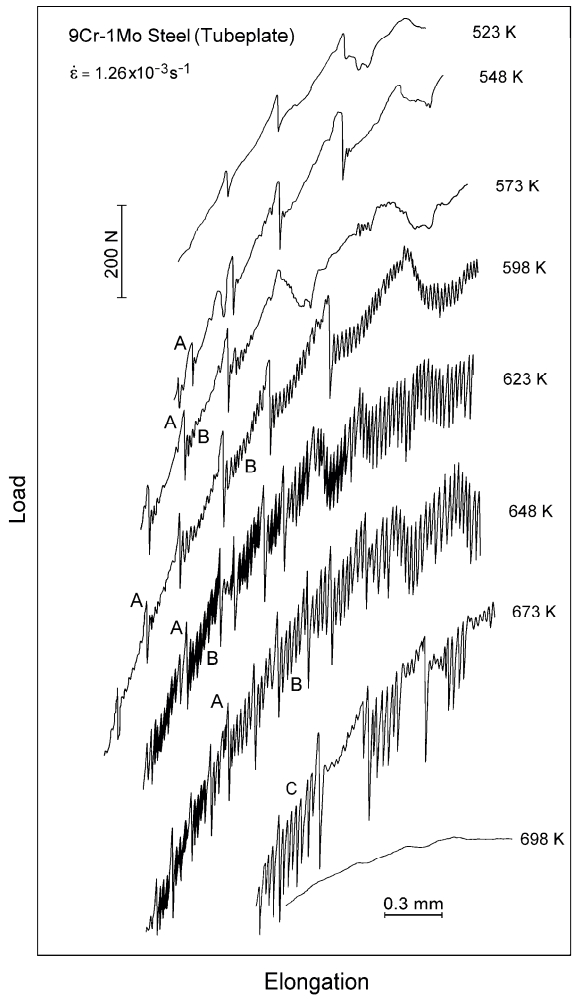

Figure 4. Segments of load-elongation curves showing serrated flow for tube plate forging at various temperatures at a strain rate of 1.26×10^{-3} s^{-1}.

est temperature of 648 K, only mild irregularities could be seen (Figure 3).

In general, the height of serrations, i.e., the magnitude of stress drops ($\Delta\sigma$) observed during serrated flow increased with increase in plastic strain and temperature (Figures 3 and 4). At a constant temperature, the strain between two successive type A serrations increased with increase in plastic strain. Different types of serrations observed for plate and tubeplate forging in the temperature range 523–698 K are summarized in Table 2. No significant difference in serrated flow temperature regime was noticed between the two product forms in 9Cr-1Mo steel. The occurrence of various types of serrations at different temperatures remained largely unaffected for both $N + T$ plate and tubeplate forging. However, in the low temperature range of serrated flow i.e., 523–598 K, tubeplate forging displayed higher propensity to serrated flow in terms of both the occurrence of higher number of type A serrations as well as larger amount

of stress drops compared to those shown by plate material at the respective temperatures (Figures 3 and 4). Further, tubeplate forging exhibited well defined type A serrations (Figure 4) compared to mild irregularities shown by $N + T$ steel (Figure 3) at 523 K.

3.3 Tensile Properties of $N + T$ Plate and Tubeplate Forging

The variations in yield strength with temperature for both $N + T$ plate and tubeplate forging are shown in Figure 5. For comparison, minimum yield strength values at different temperatures specified in ISO (International Steel Organisation) standards [16] for thin section 9Cr-1Mo steel are also given in Figure 5. The variations in ultimate tensile strength with temperature for $N + T$ plate and tubeplate forging are presented in Figure 6. Following the classification of different types of serrations [12–15] observed for plate and tubeplate forging at intermediate temperatures (Figures 3 and 4), a uniform approach for measuring load values for the evaluation of flow stress/ultimate tensile strength was adopted. For type A serrations, which showed an abrupt rise in the loads followed by discontinuous drops below the general level of load-elongation curves, general/mean levels of load values were considered. For type B serrations that oscillate about the general level of load values, mean load values were taken. For type C serrations exhibiting load drops always below the general level of load values, envelope load values were considered. The yield and ultimate tensile strength values reported for heat treatments intended to simulate thick section microstructures in bar material of 9Cr-1Mo steel [4] are superimposed in Figures 5 and 6, respectively. Sanderson and Jacques [4] used slow heating of 30 K/h to austenitising temperature of 1253 K and soaking for 16 h followed by two different transformation cooling rates of 100 K/h and 50 K/h intended to simulate the microstructures for air-cooled bar section sizes of 500 and 1000 mm, respectively. Tempering treatment involved slow heating of 30 K/h to tempering temperature of 1043 K and soaking for 2 h followed by cooling rate of 100 K/h for both 500 and 1000 mm section sizes. For transformation cooling rates of 100 K/h, tempered martensite similar to normalised and tempered steel was observed. Presence of $\sim$2% pro-eutectoid ferrite in the microstructure for transformation cooling rate of 50 K/h was observed [4]. Both yield and ultimate tensile strength values decreases gradually with increasing temperature up to an intermediate temperature followed by a rapid decrease at high temperatures (Figures 5 and 6). At all temperatures, tubeplate forging exhibited lower yield and ultimate tensile strengths compared to the strength values reported for heat treatments intended to simulate thick section microstructures as well as those

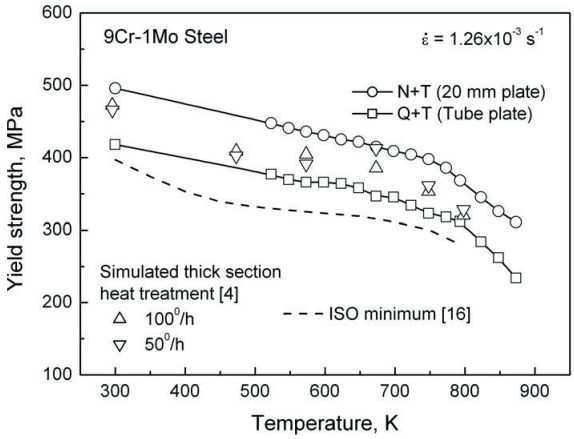

Figure 5. Variations in yield strength with temperature for $N + T$ plate and tubeplate forging. Yield strength values reported for heat treatments intended to simulate thick section microstructures and minimum yield strength values given in ISO for the steel are superimposed.

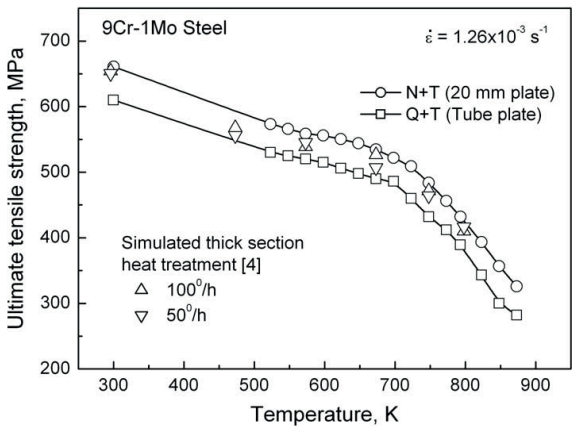

Figure 6. Variations in ultimate tensile strength with temperature for $N + T$ plate and tubeplate forging. Tensile strength values reported for heat treatments intended to simulate thick section microstructures for the steel are superimposed.

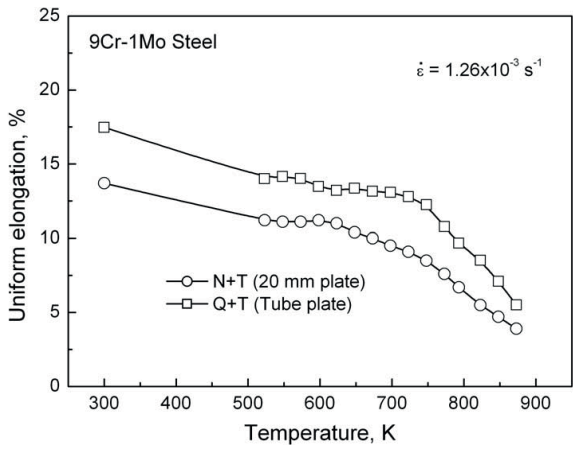

Figure 7. Variations in uniform elongation with temperature for $N + T$ plate and tubeplate forging.

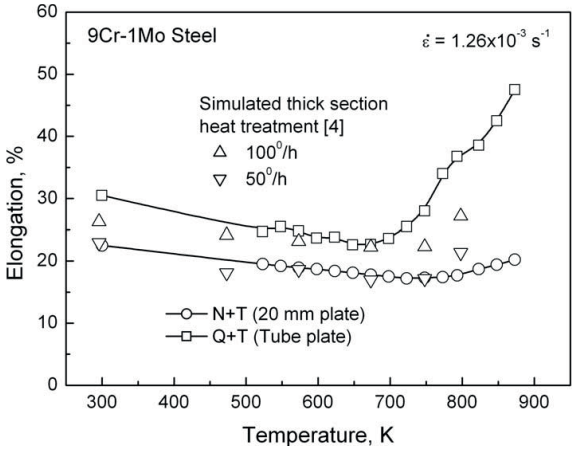

Figure 8. Variations in elongation to fracture with temperature for $N + T$ plate and tubeplate forging. Elongation values reported for heat treatments intended to simulate thick section microstructures for the steel are superimposed.

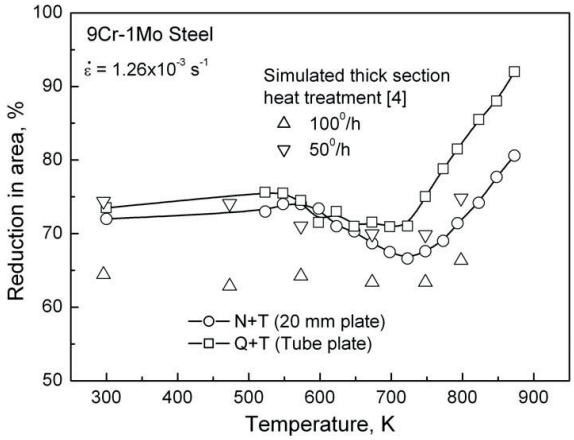

Figure 9. Variations in reduction in area with temperature for $N + T$ plate and tubeplate forging. Reduction in area values reported for heat treatments intended to simulate thick section microstructures for the steel are superimposed.

obtained for $N + T$ plate material. The yield and ultimate tensile strength values for simulated thick sections lie in between of the strength values obtained for $N + T$ plate and tubeplate forging. Further, the difference in strength values between $N + T$ plate and tubeplate forging remained nearly constant in the temperature range 300–873 K. However, the yield strength values of the forging remained higher than the minimum yield strength values given in ISO (Figure 5).

The variations in uniform elongation as a function of temperature for $N + T$ plate and tubeplate forging are shown in Figure 7. Uniform elongation comprising of elastic and plastic elongations was evaluated as the total elongation values corresponding to maximum load values in the load-elongation curves obtained from tensile tests. Uniform elongation exhibited a gradual decrease up to intermediate temperatures followed by a rapid decrease at high temperatures. At all temperatures, tubeplate forging displayed higher uniform elongation than the $N + T$ steel. The variations in elongation to fracture as a function of temperature for $N + T$ plate and tubeplate forging are shown in Figure 8. Elongation to fracture exhibited a gradual decrease to a minimum at intermediate temperatures followed by a marginal increase for $N + T$ plate material and a rapid increase for the forging at high temperatures. Tubeplate forging exhibited higher % elongation values than the $N + T$ plate at all temperatures and the increase in % elongation values was more pronounced at high temperatures. The steel with simulated thick section heat treatment conditions displayed elongation values in between of those shown by plate and tubeplate forging. No significant difference in reduction in area values for plate and tubeplate forging was noticed at room and intermediate temperatures (Figure 9). At high temperatures, tubeplate forging displayed higher reduction in area values than the plate material.

3.4 Fracture Behaviour

SEM examinations of fracture surfaces of tested specimens revealed transgranular fracture at all test conditions examined in this investigation. Transgranular fracture characterized by dimples resulting from microvoids coalescence for both $N + T$ plate and tubeplate forging are shown in Figures 10 and 11, respectively. At room and intermediate temperatures, a few chisel tip appearance resulting from the split in martensite lath boundaries at isolated locations were noticed (Figures 10a and 11a).

4 Discussion

4.1 Influence of Temperature on Tensile Properties

The gradual decrease in yield and ultimate strength values up to an intermediate temperature followed by a rapid fall at high temperatures observed for $N + T$ plate and tubeplate forging (Figures 5 and 6) is consistent with the temperature dependence of tensile strength reported for 9Cr-1Mo steel and its modified versions [1, 3, 4, 7, 17]. Serrated flow observed for both the product forms represents one of the most important manifestations of dynamic strain ageing (DSA) occurring at intermediate temperatures (Figures 3 and 4). The influence of temperature on the nature and type of serrations observed in the present investigation is in agreement with that reported for the steel and other alloy systems [19–21]. Examination on the dependence of temperature and strain rate on critical strain for the onset of serrations and evaluation of activation energy suggested that the diffusion of interstitial solutes such as carbon is responsible for serrated flow in 9Cr-1Mo steel [22]. In car-

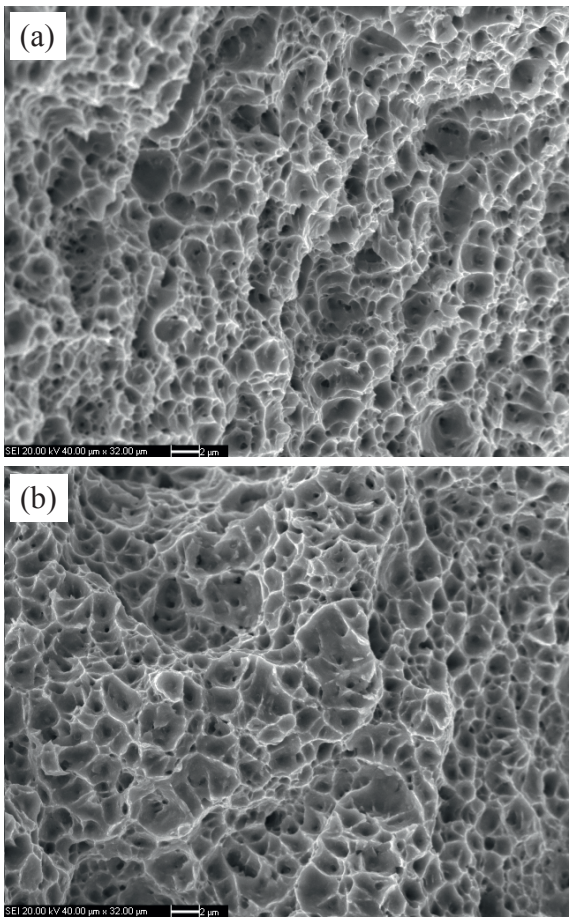

Figure 10. SEM fractographs showing transgranular fracture in $N + T$ plate specimens tested at (a) 573 and (b) 873 K. A very few chisel tip appearance can be seen in specimen tested at 573 K in (a).

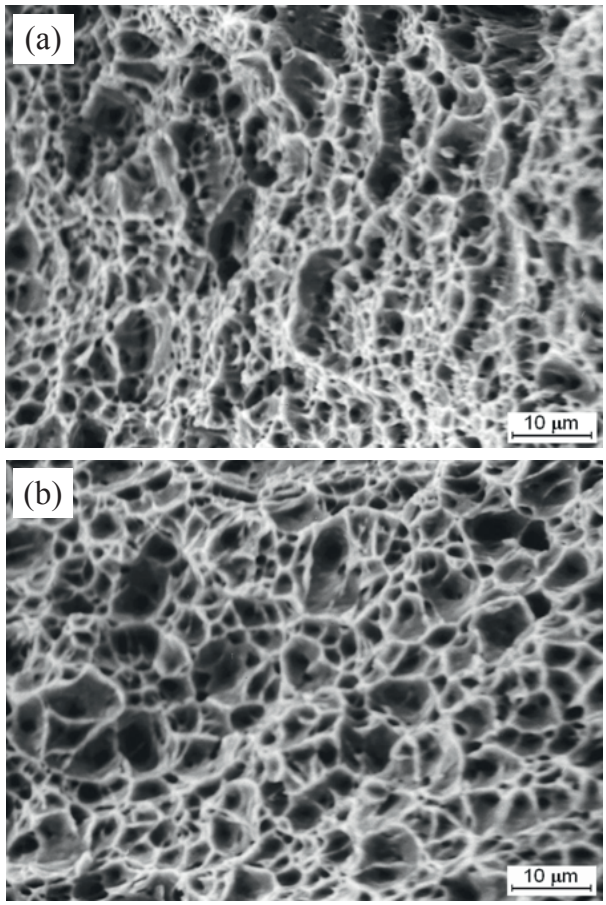

Figure 11. SEM fractographs showing transgranular fracture in tubeplate forging specimens tested at (a) 573 and (b) 873 K. A very few chisel tip appearance can be seen in specimen tested at 573 K in (a).

bon, 2.25Cr-1Mo and 9Cr-1Mo ferritic steels [23–28], locking of mobile dislocations by diffusing carbon atoms has been suggested to be the source of serrations. Increase in the height of serrations, i.e., the magnitude of stress drops with increase in plastic strain and temperature (Figures 3 and 4) indicates increased strength of solute locking of dislocations before unlocking. Mild irregularities observed in the beginning of serrated flow temperature i.e., at 523 K in Figure 3, indicate absence of sufficient amount of solutes at dislocations. Similarly, the presence of irregularities at the upper end temperature of serrated flow i.e., at 698 K in Figures 3 and 4 implies reduced propensity to dynamic strain ageing due to loss of solutes responsible for locking of dislocations to precipitate sinks such as large amount of carbides present in the steel [8–11]. The gradual decrease in strength values at intermediate temperatures rather than a rapid decrease can be ascribed to the effects associated with DSA. The influence of DSA is also manifested as the occurrence of minima in elongation to fracture and reduction in area at intermediate temperatures in both $N + T$ plate and tubeplate forging (Figures 8 and 9).

At high temperatures, both $N + T$ plate and tubeplate forging exhibited a rapid decrease in yield and ultimate tensile strength values with increasing temperature (Figures 5 and 6). Rapid decrease in strength value can arise either from coarsening of precipitates or occurrence of intergranular cracking or from the ease of deformation at high temperatures. In the short times involved in tensile tests, significant coarsening of precipitates is unlikely even at the highest test temperature. The transgranular fracture observed at all temperatures (Figures 10 and 11) rules out intergranular cracking as the possible reason for the reduction in strength values at high temperatures. Therefore, the rapid decrease in strength values can be attributed to ease of deformation due to dynamic recovery effects. At high temperatures, thermally activated processes like climb of dislocation and cross-slip would be dominant thereby enabling dynamic recovery to take place.

4.2 Comparative Evaluation of Tensile Properties between Plate and Tubeplate Forging

Tubeplate forging exhibited consistently lower yield and ultimate tensile strengths and higher ductility values than those shown by $N + T$ plate material in temperature range 300–873 K (Figures 5–9). The difference in strength values between plate and forging remained nearly constant at all temperatures. Both plate and tubeplate forging have displayed serrated flow with similar intensity in the temperature range 523–698 K. Therefore, it is unlikely that the difference in strength values observed between the two product forms of 9Cr-1Mo steel is influenced by DSA. Further, no significant difference in strength values is noticed between the two different transformation cooling rates of 100 K/h and 50 K/h used to simulate microstructures of thick sections of sizes 500 and 1000 mm, respectively, in spite of the presence of $\sim 2\%$ pro-eutectoid ferrite for cooling rate of 50 K/h (Figures 5 and 6) [4]. This suggests that there is no major effect of ferrite phase on strength values when present in small quantity. Therefore, the reduction in strength of tubeplate forging could have resulted mainly from coarse microstructure in terms of coarse prior austenite grain and martensite packet size and coarse lath martensite obtained during forging process and extended heat treatments given to tubeplate forging. Relatively high hot forging temperature and extended heat treatment of slow heating to soaking temperature and soaking for 5 h resulted in very coarse grain size of 120 μm for the forging. The observed fine austenite grain size of 25 μm in case of $N + T$ plate is comparable to the grain size in the range 20–30 μm reported for thin section 9Cr-1Mo steel austenitised in the temperature range 1223–1273 K [2,3,8]. Apart from coarse austenite grain size, the slow cooling rate experienced by the tubeplate forging due to large section size results in coarse lath martensite, which affects significantly in the reduction in strength values. Decrease in strength values with increasing grain size for hot forged product compared to hot rolled material has been reported for 9Cr-1Mo-V-Nb steel [29].

Tensile strength in 9%Cr steel is derived from fine austenitic grain and martensite packet and lath martensite size, high dislocation density and fine distribution of precipitates. In addition to coarse microstructure, tubeplate forging also exhibited coarse precipitates at the grain and lath boundaries and in the matrix regions giving rise to larger inter-barrier distance for dislocation motion during deformation (Figure 2). In order to examine the influence of overall precipitate distribution on strength values, inter-particle spacing in the plate and tubeplate forging has been evaluated using Estrin–Mecking approach [30]. In this method, constant mean free path of dislocations is defined as the mean inter-particle spacing, d. Mean inter-particle spacing is obtained from the intercept of the straight line plot of $\theta\sigma$ vs. σ^2, where θ ($\theta = d\sigma/d\varepsilon$) is the instantaneous work hardening rate. The intercept on $\theta\sigma$ axis is given by $(\alpha b^2\mu^2)/(2bd)$, where α is the dislocation length factor obtained from the relation between σ and mobile dislocation density Q_m as $\sigma = \alpha\mu b\sqrt{Q_m}$, b is Burgers vector and μ is shear modulus. Figures 12 depicts $\theta\sigma$ vs. σ^2 plots for stage-III hardening obtained from the room temperature σ-ε data for both plate and tubeplate forging. The values of intercept and corresponding inter-particle spacing for plate and tubeplate forging are given in Table 3. The d values were calculated using $\alpha = 1.3$ [23], $\mu = 82.7$ GPa [31] and $b = 2.68 \times 10^{-10}$ m [32]. The values of inter-particle spacing of 197 nm and 257 nm obtained for $N + T$ plate and tubeplate forging, respectively, are comparable to those reported for heat treated 9Cr-1Mo steel by other investigators [10, 33, 34]. The coarse precipitates seen for tubeplate forging in Figure 2 are reflected in the significantly larger inter-particle spacing of 257 nm for the forging. In addition to coarse gain, packet and lath size, large inter-particle spacing due to coarse precipitates will add in significant reduction in strength values of thick section tubeplate forging.

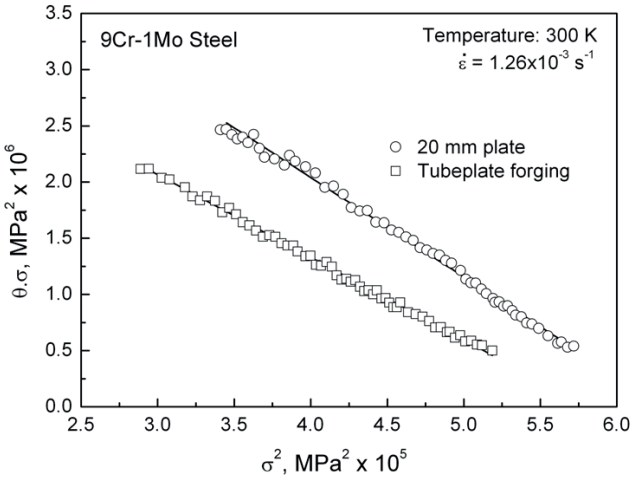

Figure 12. $\theta\sigma$ vs. σ^2 plots for stage-III hardening obtained from the true stress-true plastic strain data at room temperature for $N + T$ plate and tubeplate forging.

Product form	Intercept, MPa^2	Inter-particle spacing, nm
20 mm plate	5.58×10^6	197
Tube plate forging	4.28×10^6	257

Table 3. Values of intercept and inter-particle spacing obtained from Estrin-Mecking plots of $\theta\sigma$ vs. σ^2 obtained from true stress-true plastic strain data at room temperature for $N + T$ plate and tubeplate forging.

5 Concusion

Both $N + T$ plate and thick section tubeplate forging exhibited a gradual decrease in yield and ultimate tensile strengths with increase in temperature up to intermediate temperatures followed by a rapid decrease at high temperatures. Elongation and reduction in area displayed a gradual decrease to minima at intermediate temperatures followed by rapid increase at high temperatures. Serrated flow, a manifestation of dynamic strain ageing was observed at intermediate temperatures. Both plate and forging exhibited transgranular fracture. At all temperatures, tubeplate forging exhibited lower strength and higher ductility values than those shown by plate material. The inferior strength of tubeplate forging is ascribed to the effects associated with coarseness of microstructure in terms of coarse austenite grain, martensite packet and lath martensite size and precipitates.

References

[1] D. S. Wood, A. B. Baldwin, F. W. Grounds, J. Wynn, E. G. Wilson and J. Waring, *Ferritic Steels for Fast Reactor Steam Generators*, S. F. Pugh and E. A. Little (eds.), 1977, pp. 189–192. British Nuclear Energy Society, London.

[2] B. J. Cane and R. S. Fidler, *Ferritic Steels for Fast Reactor Steam Generators*, S. F. Pugh and E. A. Little (eds.), 1977, pp. 193–199. British Nuclear Energy Society, London.

[3] E. Barker, G. J. Lloyd and R. Pilkington, *Mater Sci. Eng.*, **84**, 49 (1986).

[4] S. J. Sanderson and S. Jacques, *Proc. IAEA Specialist Meeting on Mechanical Properties of Structural Materials Including Environmental Effects*, 1983, Report IWGFR-49, 1984, Vol. 2, pp. 601–611, Chester, England.

[5] J. A. Seran, A. Alamo, A. Maillard, H. Touron, J. C. Brachet, P. Dubuisson, D. Gilbon and O. Rabouille, *J. Nucl. Mater*, **212–215**, 588 (1994).

[6] A. Alamo, J. L. Bertin, V. K. Shamardin and P. Wident, *J. Nucl. Mater*, **367–370**, 54 (2007).

[7] K. Laha, K. S. Chandravathi, K. B. S. Rao and S. L. Mannan, *Inter J. Pres. Ves. Piping*, ***62***, 303 (1995).

[8] S. J. Sanderson, *Met. Sci. J.*, **11**, 490 (1977).

[9] M. Wall, B. C. Edwards and J. A. Hudson, *Proc. IAEA Specialist Meeting on Mechanical Properties of Structural Materials Including Environmental Effects*, 1983, Report IWGFR-49, 1984, Vol. 2, pp. 545–577, Chester, England.

[10] B. A. Senior, F. W. Noble and B. L. Eyre, *Acta Metall*, **34**, 1321 (1986).

[11] C. A. Hippsley and N. P. Haworth, *Mater Sci Technol*, **4**, 791 (1998).

[12] B. Russel, *Philos Mag*, **8**, 615 (1963).

[13] A. J. R. Solar Gomez and W. J. Mc Tegart, *Philos Mag*, **20**, 495 (1969).

[14] E. Pink and A. Grinberg, *Mater Sci Eng*, **51**, 1 (1981).

[15] P. Rodriguez, *Encyclopedia of Materials Science and Engineering*, R. W. Cahn (ed.), 1988, Supplimentry Vol. 1, pp. 504–508, Pergamon Press, Oxford.

[16] International Standard ISO 2604, Steel products for pressure purposes and quality requirements, 1975, International Standards Organisation.

[17] V. K. Sikka, *Ferritic Alloys for Use in Nuclear Energy Technologies*, J. W. Davies and D. J. Michael (eds.), 1984, pp. 317–327. TMS-AIME, Warrendale, Pa.

[18] B. J. Brindley and P. J. Worthington, *Metall Rev*, **145**, 101 (1970).

[19] S. L. Mannan, K. G. Samuel and P. Rodroguez, *Trans Indian Inst Met*, **36**, 313 (1983).

[20] K. B. S. Rao, V. Seetharaman, S. L. Mannan and P. Rodriguez, *High Temp Mater Proc*, **7**, 63 (1986).

[21] K. Laha, K. S. Chandravathi, K. B. S. Rao and S. L. Mannan, *Z Metallkd*, **2**, 839 (1994).

[22] B. K. Choudhary, V. S. Srinivasan and M. D. Mathew, Mater. High Temp, **28**, 155 (2011).

[23] A. S. Keh, Y. Nakada, and W. C. Leslie, *Dislocation Dynamics*, A. R. Rosenfield (ed.), 1968, pp. 381–408, McGraw-Hill, New York.

[24] J. D. Baird, *Metall Rev*, **149**, 1 (1971).

[25] P. G. Mccormick, *Acta Metall*. **21**, 873 (1973).

[26] R. W. Hayes and W. C. Hayes, *Acta Metall*, **32**, 259 (1984).

[27] R. K. Upadhyaya and M. N. Shetty, *Z Metallkd*, **82**, 19 (1991).

[28] A. K. Roy, P. Kumar and D. Maitra, *Mater Sci Eng A*, ***499***, 379 (2009).

[29] G. Ebi and A. J. Mc Evily, *Fat Fract Eng Mater Struct*, **7**, 229 (1984)

[30] Y. Estrin and H. Mecking, *Acta Metall*, **32**, 57 (1984)

[31] Design and Construction Rules for Mechanical Components of FBR Nuclear Islands. (2002) RCC-MR, Section 1, Subsection Z, Appendix A3.18S.22.

[32] R. Schaublin, P. Spatig and M. Victoria, *J Nucl Mater*, **258–263**, 1178 (1998).

[33] B. A. Senior, F. W. Noble and B. L. Eyre, *Acta Metall*, **36**, 1855 (1988).

[34] A. Moitra, P. R. Sreenivasan, P. Parameswaran and S. L. Mannan, *Mater Sci Technol*, **18**, 1985 (2002).